

Copyright 1997 Society of Photo-Optical Instrumentation Engineers. This paper was published in *Proceedings of SPIE* and is made available as an electronic reprint with permission of SPIE. One print or electronic copy may be made for personal use only. Systematic or multiple reproduction, distribution to multiple locations via electronic or other means, duplication of any material in this paper for a fee or for commercial purposes, or modification of the content of the paper are prohibited.

101-frame algorithm for phase shifting interferometry

Peter de Groot

zygo, Laurel Brook Road, Middlefield, CT USA 06455

INTRODUCTION

Phase shifting interferometry (PSI) is one of the more common techniques for interpolation between interference fringes. A surface-profiling PSI instrument stores CCD image frames of fringe patterns for a series of reference phases; then applies a mathematical algorithm to recover phase information.¹ Because the wavefront phase itself is a linear function of the surface profile, PSI provides a high-resolution measurement of the surface figure.

In the early days, computational limits restricted the number of image frames to three or four, which does not leave much room for variation. As demands for precision have increased, so have the length and variety of phase-shifting algorithms. The state of the art has advanced to 5, 7 and even 15 frame varieties. At the same time, the level of sophistication in deriving these algorithms has risen dramatically.^{2,3,4} This paper explores the limits of these trends, while reviewing some of the mathematical techniques that we at Zygo use to analyze PSI performance. Finally, in an attempt to predict far into the future, I present a 101-frame algorithm that is highly resistant to error sources. This somewhat extreme example highlights the practical limits on algorithm length, which are actually more relaxed than one might think, provided that we loosen the definition of PSI.

FUNDAMENTALS OF PSI

Estimation of a wavefront phase θ in PSI requires $N \geq 3$ interference images or camera frames, each having a different phase offset ϕ_j , where $j = 0..N - 1$. For practical reasons and for ease in the data processing, the phase shifts ϕ_j are typically linear in time and have a constant phase increment α_0 . For a given pixel in the field of view, the intensity samples are

$$g_j = Q \left[1 + V \cos(\theta + \phi_j) \right], \quad (1.)$$

where V is the fringe visibility, Q is a constant and

$$\phi_j = (j - j_0)\alpha_0. \quad (2.)$$

PSI algorithms for calculating the phase θ are of the form

$$\theta = \tan^{-1} \left(\frac{\sum s_j g_j}{\sum c_j g_j} \right) + \text{const.}, \quad (3.)$$

where s_j and c_j are constant coefficients. For example, a popular algorithm using an $\alpha_0 = \pi/2$ phase step is the five-frame Schwider-Hariharan algorithm.^{5,6}

$$\theta = \tan^{-1} \left(\frac{2(g_1 - g_3)}{2g_2 - (g_0 + g_4)} \right). \quad (4.)$$

The non-zero coefficients in this case are $s_1 = 2$, $s_3 = -2$, $c_0 = -1$, $c_2 = 2$ and $c_4 = -1$.

SAMPLING WINDOW MODEL

PSI processing can be interpreted as a discrete Fourier transform (DFT)⁷ combined with a data sampling window.⁸ From the DFT point of view, the phase θ is calculated from the argument of the Fourier Transform G of the intensity signal g , where G is given by

$$G = \sum_j g_j w_j \exp(-i\phi_j). \quad (5.)$$

The weighting values w_j correspond to the sampling window. An important class of algorithms employs real, symmetric windows, for which the algorithm coefficients work out to be

$$s_j = w_j \sin(-\phi_j) \quad (6.)$$

$$c_j = w_j \cos(\phi_j). \quad (7.)$$

For the Schwider-Hariharan PSI algorithm, $w_1 = w_2 = w_3 = 2$ and $w_0 = w_4 = 1$. Table 1 below includes several additional examples.

The sampling-window model provides a means of deriving new algorithms as well as an insight into error sources. Error-compensating algorithms are approximately bell-shaped when represented graphically (Figure 1).⁹ Such a window reduces the effects of negative-frequency leakage in the Fourier domain. The practical consequence is that these algorithms are more robust in the presence of phase-shift calibration errors and mechanical vibrations.

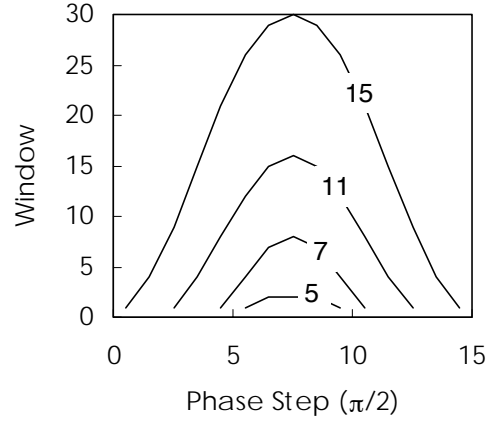


Figure 1: Sampling windows for PSI algorithms having 5 to 15 frames.

Table 1: PSI algorithms having real, symmetric data sampling windows

N	w	$\tan^{-1}(\theta)$
4	[1, 1, 1, 1]	$\frac{g_0 - g_2}{g_3 - g_1}$
5	[1, 2, 2, 2, 1]	$\frac{2(g_1 - g_3)}{-(g_0 + g_4) + 2g_2}$
7	[1, 4, 7, 8, 7, 4, 1]	$\frac{-(g_0 - g_6) + 7(g_2 - g_4)}{-4 \cdot (g_1 + g_5) + 8 \cdot g_3}$
11	[1, 4, 8, 12, 15, 16, 15, ...]	$\frac{(g_0 - g_{10}) - 8(g_2 - g_8) + 15(g_4 - g_6)}{4(g_1 + g_9) - 12(g_3 + g_7) + 16g_5}$
15	[1, 4, 9, 15, 21, 26, 29, 30, 29, ...]	$\frac{-(g_0 - g_{14}) + 9(g_2 - g_{12}) - 21(g_4 - g_{10}) + 29(g_6 - g_8)}{-4(g_1 + g_{13}) + 15(g_3 + g_{11}) - 26(g_5 + g_9) + 30g_7}$

RESISTANCE TO CALIBRATION ERRORS

Since PSI algorithms are designed for specific phase increments, they cannot be expected to perform perfectly if the increment is incorrect. Suppose that instead of the assumed phase shifts α_0 as in Eq.(2.), we have

$$\alpha = (1 - \varepsilon) \alpha_0, \quad (8.)$$

where α is the actual phase increment and ε is the calibration error. The calibration error ε is a function of a number of different experimental parameters, some of which cannot be controlled or entirely eliminated by calibration procedures. These parameters include tilting or twisting of the PZT pusher during translation, and geometrical effects that arise when working with fast spherical cavities.

Using the window model, it is possible to derive an exact, analytical formula for the peak-to-valley (PV) error resulting from calibration errors.¹⁰ The result is

$$E(\varepsilon) = 2 \tan^{-1} \left(\frac{W_2(\varepsilon)}{\sqrt{W_0(\varepsilon)^2 - W_2(\varepsilon)^2}} \right). \quad (9.)$$

where

$$W_0(\varepsilon) = \left| \frac{W(\varepsilon \alpha_0)}{W(0)} \right| \quad (10.)$$

$$W_2(\varepsilon) = \left| \frac{W((2 - \varepsilon) \alpha_0)}{W(0)} \right| \quad (11.)$$

and

$$W(\alpha) = \sum_j w_j \exp(-i\phi_j \alpha/\alpha_0) \quad (12.)$$

is the Fourier transform of the data sampling window w . Eq.(9) is an exact formula for the P-V error, valid for all PSI algorithms having the form of Eq.(3).

It turns out that the effect of calibration errors is strongly dependent upon the choice of algorithm. It appears from Figure 2 that a well-constructed algorithm with a large number of sample frames can eliminate calibration error as a source of concern.

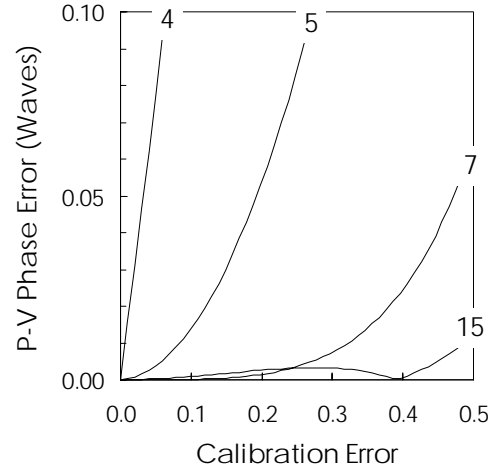


Figure 2: Phase-step calibration errors for the 4,5,7 and 15-frame algorithms listed in Table 1.

VIBRATION

Of course, phase step calibration is not the only source of error. During a PSI acquisition, mechanical vibrations $n(t)$ disturb the phase shifts and add noise to the intensity signal. One way to analyze the resultant errors is to consider the effect of pure vibrational tones of frequency ν , amplitude A and phase offset α . In that case,

$$n(t) = A \cos(2\pi\nu t + \alpha). \quad (13.)$$

It is possible to calculate the error for these pure tones analytically, in a linear approximation.¹¹ For a real, symmetric data sampling window w , the calculation involves the following transforms:

$$\begin{aligned} F_S(\nu) &= \frac{1}{q} \sum_j w_j \sin(-\phi_j) \exp(-i\phi_j \nu) \\ F_C(\nu) &= \frac{1}{q} \sum_j w_j \cos(\phi_j) \exp(-i\phi_j \nu) \end{aligned} \quad (14.)$$

where

$$q = \sum_j w_j \sin^2(\phi_j) = \sum_j w_j \cos^2(\phi_j) \quad (15.)$$

Then the rms error for vibrations of random phase is then¹²

$$E'(\nu) = \frac{A\sqrt{2}}{8} \left| i \left[F_S^*(\nu+1) + F_C^*(\nu-1) \right] - \left[F_S^*(\nu-1) + F_C^*(\nu+1) \right] \right|. \quad (16.)$$

The frequency ν is normalized to the data acquisition rate ν_0 , which for $\pi/2$ algorithms is 1/4 the camera rate.

Figure 2 shows the vibrational response for the 3-, 7- and 15-frame algorithms. The smaller the area under the curve, the better, particularly in the low-frequency region. There is once again a clear improvement with increased frame number. With fifteen frames, there is zero sensitivity to small vibrations (< tenth fringe) up to a normalized frequency of 1.2. For a 60-Hz CCD camera, this corresponds vibration immunity up to 18Hz. Large amplitude vibrations generate a somewhat different response, although the same improvement trend with algorithm size is preserved.¹³

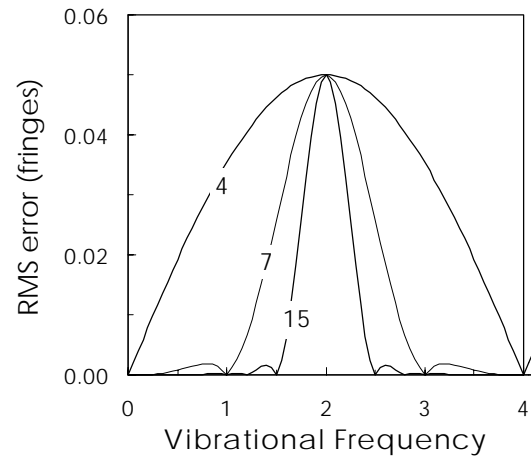


Figure 3: Phase-measurement errors for the 5,7 and 15-frame algorithms, for a vibrational amplitude equivalent to 0.1 rad.

THE ULTIMATE, 101 FRAME ALGORITHM?

There are many other sources of error that can be quantified with the window model and Fourier analysis. These include random intensity noise, nonlinear phase shifts, harmonic signal noise and so on. For all of these error sources, there is a common, clear trend: the larger the number of CCD frames, the easier it is to suppress errors. Given enough computing power, it should be practical to store and process dozens of computer frames each having a million pixels.

So why not speculate about a really big algorithm, having, say, 101 frames? It is easy enough to derive such an algorithm using the sampling window concept. An appropriate 101-coefficient symmetric window is

$$w = [\begin{matrix} 1 & 3 & 7 & 12 & 19 & 27 & 37 & 48 & 60 & 74 & 88 \\ 104 & 122 & 140 & 159 & 179 & 200 & 222 & 244 & 267 & 291 & 314 \\ 339 & 363 & 388 & 412 & 437 & 461 & 486 & 509 & 533 & 556 & 578 \\ 600 & 621 & 641 & 660 & 678 & 696 & 712 & 726 & 740 & 752 & 763 \\ 773 & 781 & 788 & 793 & 797 & 799 & 800 & 799 & 799 & \dots &] \end{matrix}$$

This window, together with a standard DFT as described in previous sections, provides a very high resistance to errors. For example, the small-amplitude vibration sensitivity for the “101” is reduced to a very small frequency region (Figure 4). The algorithm is virtually insensitive to vibration.

In spite of these positive results, the practicality of very long PSI algorithms is in doubt. For one thing, the phase-shifting mechanism must be able to cope with a phase range of several hundred radians. Furthermore, interference microscopes that employ PSI often have a coherence depth that is too short for a 101-frame algorithm.

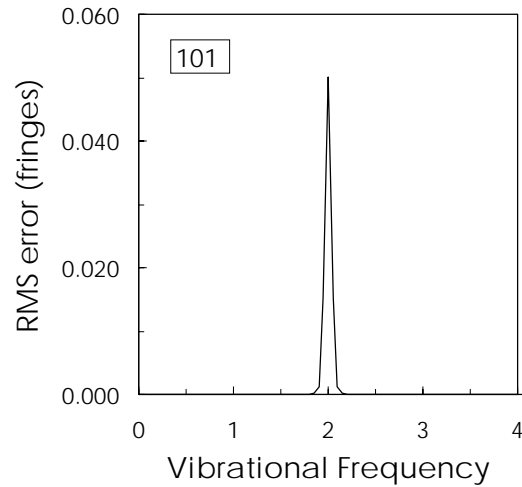


Figure 4: Phase-measurement errors for the 101-frame algorithm, for a vibrational amplitude equivalent to 0.1 rad. Compare with Fig.3.

There is even a more fundamental problem with very long PSI, related to the uniformity and calibration of the phase shift. This becomes evident when calculating the effective fringe contrast or signal strength as a function of calibration error. It can be shown that the signal strength V' is given by the formula

$$V'(\varepsilon) = V W_0(\varepsilon) \quad (17.)$$

where W_0 was defined in Eq.(10), and V is the fringe contrast. Figure 5 compares the signal strength for three different algorithms, including the 101, for $V=1$. The 101-frame algorithm is

obviously severely constrained. This makes very long PSI algorithms such as this one quite fragile. Thus, in spite of my hopes of deriving the ultimate algorithm, I think we will be doing PSI with fewer than 101 frames for quite a while.

LONG-SCAN PSI THAT WORKS

In light of these difficulties, it may come as a surprise that very large PSI algorithms are already in use. A known form of measuring microscope employs white light and frequency-domain analysis (FDA).¹⁴ An FDA instrument collects 64 frames of interferograms during a continuous phase shift, generated by mechanical translation of an Mirau objective. These interference data are transformed pixel-by-pixel into the spatial frequency domain by Fourier analysis. The transform is equivalent to applying a half-dozen, 64-frame PSI algorithms to each pixel.

The loss of signal strength is not an issue in FDA with its 64-frame analysis, because there is no *a priori* assumption regarding the size of the phase increment α_0 . The Fourier transform in FDA covers a range of spatial frequencies corresponding to a range of phase increments. One of these frequencies always has a high signal strength, and this is the frequency used for the final phase analysis. To provide the range of spatial frequencies, the instrument operates with broad-band illumination, i.e. white light. The white-light fringes shown in Figure 6 have the characteristic that they are already modulated by what amounts to a data-sampling window, also known as the coherence envelope. Thus the individual PSI algorithms for each spatial frequency are particularly simple: they are bundled together into an ordinary Fast Fourier Transform. The FDA technique enjoys all of the advantages of error reduction characteristic of long-scan PSI, without the constraint of precise calibration.

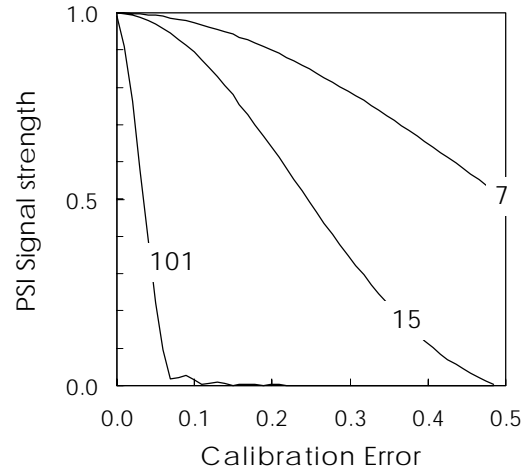


Figure 5: Decline in signal strength with calibration error for the 7,15 and 101--frame algorithms. The 101 requires precise calibration to maintain high signal strength.

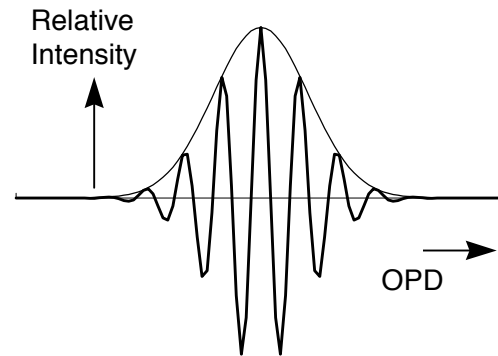


Figure 6: Frequency-domain analysis of white-light fringes such as these may be considered a special form of long-scan PSI. This kind of PSI is in widespread use today.

CONCLUSION

The art of PSI has matured greatly in the past few years, and we now have much greater flexibility in the size and shape of phase-estimation algorithm. One direction for further research is in very long algorithms, to reduce sensitivity to a variety of error sources. However, such algorithms, although easily derived, must contend with the fundamental limits of coherence and calibration.

I have successfully derived a 101-frame algorithm of the conventional type, and have calculated the improvement in error resistance. I have also shown that a very-long PSI algorithm it is not very practical. However, it is noteworthy that long-scan PSI with white-light illumination is not only feasible, but in fact has been a commercial product for several years.¹⁵ For the special case of white-light interferometry, Frequency-domain analysis of the interference pattern provides a kind of adaptive data processing that breaks through the length barrier of conventional PSI algorithms. Perhaps in the near future, a more general type of PSI instrument could be designed that maintains these benefits without restricting the system to white light.

REFERENCES AND NOTES

- ¹ P. Hariharan, *Optical Interferometry* (Academic Press, Orlando, Florida, 1985), Chap.9, pp.155-159.
- ² K. Freischlad and C. L. Koliopoulos, "Fourier description of digital phase-measuring interferometry," *J. Opt. Soc. Am. A* 7(4), 542-551 (1990).
- ³ K. Hibino, B. F. Oreb, D. I. Farrant and K. G. Larkin, "Phase-shifting algorithms for nonlinear and spatially nonuniform phase shifts," *J. Opt. Soc. Am.* 14(4), 918-930 (1997).
- ⁴ Y. Surrel, "Design of algorithms for phase measurements by the use of phase stepping," *Appl. Opt.* 35, 51-60 (1996).
- ⁵ J. Schwider, R. Burow, K.-E. Elssner, J. Grzanna, R. Spolaczyk and K. Merkel, "Digital wave-front measuring interferometry: some systematic error sources," *Appl. Opt.* 22(21), 3421-3432 (1983).
- ⁶ P. Hariharan, B.F. Oreb, and T. Eiju, "Digital phase-shifting interferometry: a simple error-compensating phase calculation algorithm," *Appl. Opt.* 26(13), 2504-2506 (1987).
- ⁷ J. H. Bruning, D. R. Herriott, J. E. Gallagher, D. P. Rosenfeld, A. D. White, and D. J. Brangaccio, "Digital wavefront measuring interferometer for testing optical surfaces and lenses," *Appl. Opt.* 13(11), 2693-2703 (1974).
- ⁸ P. de Groot, "Derivation of phase shift algorithms for interferometry using the concept of a data sampling window," *Appl. Opt.* 34(22) 4723-4730 (1995).
- ⁹ J. Schmit and K. Creath, "Window function influence on phase error in phase-shifting algorithms," *Appl. Opt.* 35(28), 5642-5649 (1996).

- ¹⁰ P. de Groot, "Phase-shift calibration errors in interferometers with spherical Fizeau cavities," *Appl. Opt.* **34**(16) 2856-2862 (1995).
- ¹¹ P. de Groot, "Vibration in phase shifting interferometry," *J. Opt. Soc. Am. A* **12**(2), 354-365 (1995).
- ¹² These vibration equations are for phase stepping algorithms, which do not involve the "integrating bucket" technique. The more general case is treated in detail in the cited references.
- ¹³ P. de Groot and L. Deck, "Numerical simulations of vibration in phase shifting interferometry," *Appl. Opt.* **35**(13), 2172-2178 (1996).
- ¹⁴ P. de Groot and Leslie Deck, "Surface profiling by analysis of white-light interferograms in the spatial frequency domain," *J. Mod. Opt.* **42**(2), 389-401 (1995).
- ¹⁵ Product literature, Zygo NewView 200 Surface Structure Analyzer. US Patent Nos. 5,398,113 and 5,402,234.